

Monometallic Catalytic Models Hosted in Stable Metal–Organic Frameworks for Tunable CO₂ Photoreduction

Xiao-Kun Wang,^{†,‡} Jiang Liu,^{‡,§} Lei Zhang,[‡] Long-Zhang Dong,^{‡,§} Shun-Li Li,[‡] Yu-He Kan,[§] Dong-Sheng Li,^{*,†,§} and Ya-Qian Lan^{*,‡,§}

[†]College of Materials and Chemical Engineering, Key Laboratory of Inorganic Nonmetallic Crystalline and Energy Conversion Materials, China Three Gorges University, No. 8, Daxue Road, Yichang 443002, P.R. China

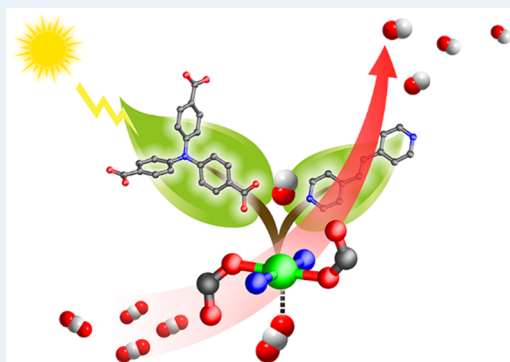
[‡]School of Chemistry and Materials Science, Jiangsu Key Laboratory of Biofunctional Materials, Nanjing Normal University, Nanjing 210023, P.R. China

[§]Jiangsu Province Key Laboratory for Chemistry of Low-Dimensional Materials, School of Chemistry and Chemical Engineering, Huaiyin Normal University, Huai'an 223300, P.R. China

Supporting Information

ABSTRACT: The photocatalytic reduction of CO₂ to energy carriers has emerged as one of the most promising strategies to alleviate the energy crisis and CO₂ pollution, for which the development of catalyst was considered as the determining factor for the accomplishment of this conversion process. In this study, three stable and isostructural metal–organic frameworks (denoted as MOF-Ni, MOF-Co, and MOF-Cu) have been synthesized and used as heterogeneous catalysts in photocatalytic CO₂ reduction reaction (CO₂RR). It is worth noting that the MOF-Ni exhibited very high selectivity of 97.7% for photoreducing CO₂ to CO, which has exceeded most of the reported MOF-based catalysts in the field. Significantly, the MOFs associated with a monometallic catalytic center offer a simple and precise structural model which allows us to understand more definitively the specific effects of different metal-ion species on photoreduction of CO₂ as well as the reactive mechanism.

KEYWORDS: metal–organic frameworks, isostructural, photocatalytic CO₂ reduction, high selectivity, monometallic catalytic model, reactive mechanism



In recent years, the increased emission of anthropogenic CO₂ from the burning of fossil fuels is leading to serious issues such as global warming and an energy crisis. Great efforts in finding efficient strategies to solve these problems have been made.^{1,2} For instance, considering that solar energy is a clean and renewable energy source, visible-light-driven photocatalytic CO₂ reduction reaction (CO₂RR) that converts CO₂ into carbon-based energy carriers (hydrocarbon fuels or chemicals) has been considered as one of the most promising solutions.^{3–6} However, the activation process for the CO₂ molecule with intrinsic chemical inertness that enables the reaction to overcome large thermodynamic barriers is difficult to achieve. Fortunately, the development of efficient and selective catalysts has proven to be extremely vital in addressing the above issue. In recent years, a variety of semiconductors (e.g., TiO₂, ZrO₂, Bi₂WO₆, and WO₃) and nanocomposites have been used as photocatalysts to attain CO₂RR.^{7–11} Although most semiconductor-based nanomaterials exhibit high photocatalytic performance, the complicated structural components and indistinct active sites are always difficult to productively investigate the reactive mechanism.^{12–15} Consequently, how to develop an efficient photo-

catalyst with precise structural information in principle is an important prerequisite for an explanation of the photocatalytic mechanism of CO₂RR.¹⁶

Metal–organic framework (MOF) constructed by metal ions/clusters and functionalized organic ligands is a one kind of crystalline material with well-defined structure. Because of the structural tailorability and ultrahigh surface area, MOF has been widely applied in many fields.^{17–31} Recently, many studies have demonstrated that MOFs can serve as catalysts to reduce CO₂ as well as offer a good platform to study the reaction mechanism on a molecular level; interest in this area of research continues to increase.^{32–41} However, the reaction condition for CO₂ photoreduction is somewhat harsh in that it usually requires the catalyst to have high structural stability in reaction solution. This is actually a big challenge for the majority of the reported crystalline MOFs. In particular, the CO₂RR carried out in a relatively alkaline system, which is beneficial for the dissolution of more CO₂, has additional

Received: December 6, 2018

Revised: January 12, 2019

Published: January 15, 2019

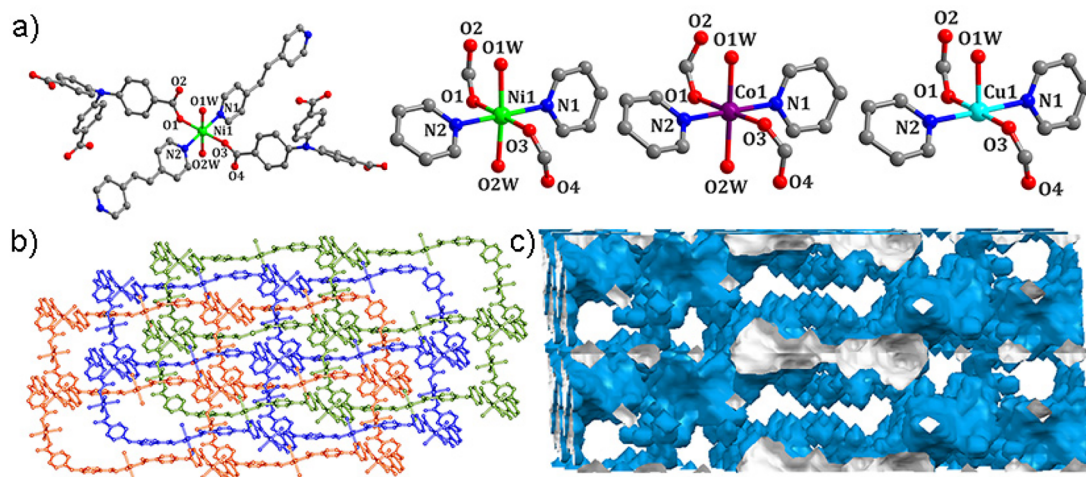


Figure 1. (a) Coordination environment of MOFs. (b) Schematic view of the threefold interpenetrating layer. (c) 3D channel simulated diagram of MOF-Ni.

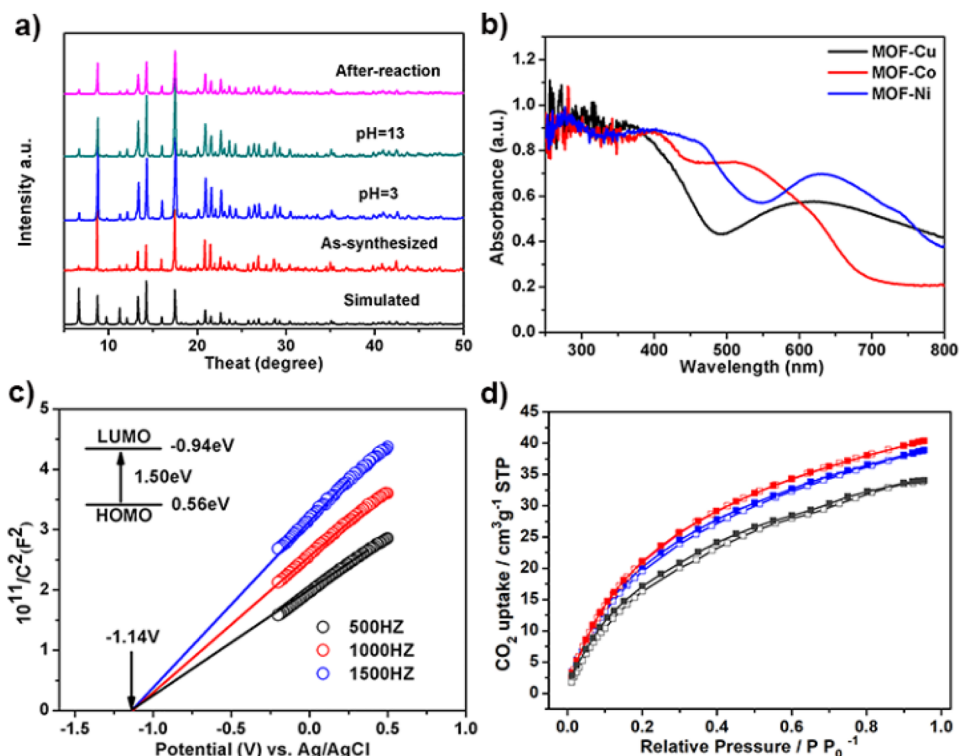


Figure 2. (a) PXRD patterns of MOF-Ni. (b) UV-vis spectra of MOF-Ni (blue), MOF-Cu (black), and MOF-Co (red). (c) Mott-Schottky plots for MOF-Ni in 0.2 M Na₂SO₄ aqueous solution. (d) CO₂ adsorption behavior for MOF-Co (red) as well as MOF-Ni (blue) and MOF-Cu (black) at 298 K.

requirements for chemical stability of the involved MOF. Additionally, the active centers of most MOF-based catalysts are mainly homo-/heterometallic cluster as secondary building units.^{42–44} Because of the collaborative contribution and interaction between active centers within a cluster to the photocatalytic performance, the catalytic ability of a single-metal active site is hard to evaluate such that the relevant reaction mechanism is still elusive and intricate.^{45–47} Consequently, the construction of MOF-based catalyst with a single catalytic active center and high structural robustness to overcome the aforementioned troubles is quite desirable.

With these considerations in mind, we successfully designed and synthesized three stable and isomorphous MOFs, {Cu₃(TCA)₂(dpe)₃(H₂O)₃}_n (MOF-Cu), {Co₃(TCA)₂(dpe)₃(H₂O)₆}_n (MOF-Co), and {Ni₃(TCA)₂(dpe)₃(H₂O)₆}_n (MOF-Ni), which are used in different transition-metal centers (Cu^{II}, Co^{II}, and Ni^{II}) and mixed organic ligands [4,4',4''-nitrilotribenzoic acid ligands (TCA) and 1,2-di(4-pyridyl)ethylene (dpe)]. It is noteworthy that these MOFs use a single active metal center as a node, which implies a simple and straightforward structural model to analyze the influence of different transition-metal centers on photocatalytic reduction of CO₂. As expected, the MOFs with

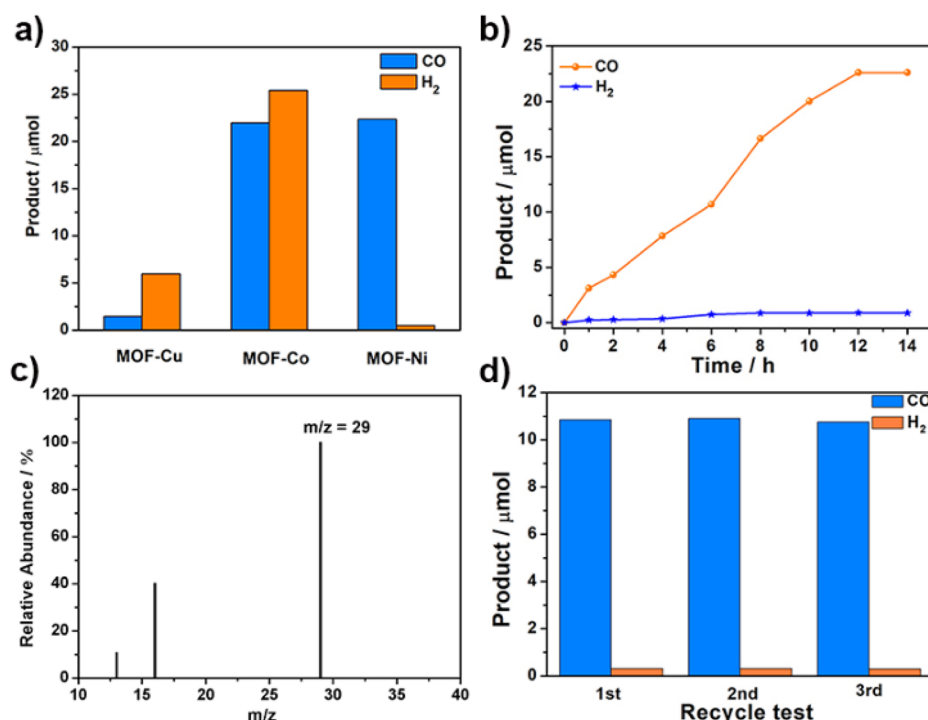


Figure 3. (a) Photocatalytic production of CO and H₂ catalyzed by MOF-Cu, MOF-Co, and MOF-Ni. (b) Amount of CO and H₂ produced as a function of the time of visible-light irradiation over MOF-Ni. (c) Mass spectra ($m/z = 29$) analysis of the source of CO. (d) The recycle experiments of MOF-Ni.

different catalytic active centers (Cu^{II}, Co^{II}, and Ni^{II}) were treated as catalysts applied in heterogeneous photocatalytic CO₂RR, which indeed resulted in notable effects on the sort and selectivity of mainly reductive products. Interestingly, MOF-Ni exhibited very high catalytic selectivity (97.7%) of CO, which has surpassed most of the reported MOF-based catalysts applied in photocatalytic CO₂RR, representing the most efficient MOF-based catalyst with Ni^{II} ion as the active center. By contrast, MOF-Cu and MOF-Co showed high selectivity (77.4%) of H₂ and moderate selectivity (47.4%) of CO, respectively. Notably, the corresponding theoretical calculations are consistent with the favorable photocatalytic results and offer important insight into the influence of different monometallic catalytic centers on photocatalytic CO₂ conversion.

Single-crystal X-ray diffraction analysis reveals that MOF-Cu, MOF-Co, and MOF-Ni have almost identical host frameworks; all of them crystallize in the trigonal system with $R\bar{3}$ space group. The only difference is that five-coordinated Cu^{II} ion adopts tetragonal pyramid geometry, while Co^{II} and Ni^{II} ions have one more axial coordination H₂O molecule to form an octahedron environment (Figure 1a, Figures S1 and S2). The coordination sphere of Cu^{II} ion is surrounded by two carboxylate-O atoms from two TCA ligands, two N atoms from two dpe ligands, and one O atom from axial coordination H₂O molecule. Considering that MOF-Co and MOF-Ni are isomorphous, MOF-Ni is selected to describe their structures herein. MOF-Co and MOF-Ni include two equivalent pairs of N and O atoms, the same as the Cu^{II} ion in the equatorial plane and two O atoms from two axial coordination H₂O molecules. The Ni–N/O bond lengths in the equatorial plane are in the range of 2.0–2.1 Å, while the axial Ni–O bond lengths are 2.0 Å.^{48–50} The carboxylate group of the TCA ligand adopts a $\mu^1-\eta^1:\eta^0$ coordination mode

and each TCA ligand connects three different Ni^{II} ions (Figure S3a). Notably, TCA ligands are connected to Ni ions along the crystallographic c axis to form a 2D network having a twisted hexagon window (Figure S3b), and 2D networks are threefold interpenetrated into a layered structure (Figure 1b). Interestingly, the adjacent 2D layers are further pillared by the dpe ligands to form an overall 3D network (Figure 1c and Figure S4). Additionally, the framework of MOF-Ni and MOF-Co can be described as 3,4-connected networks with the Schläfli symbol $\{10^3\}^2\{10^6\}^3$ from topology (Figure S5).

The purity of the as-synthesized crystals was verified by a powder X-ray diffraction (PXRD) pattern that matched well with the simulated one from the crystal structure (Figure 2a, Figures S7 and S8). It was determined that these MOFs exhibit good chemical stabilities that can maintain their structures in a broad pH value range. Furthermore, their high thermal stabilities were also verified by the thermogravimetric (TG) curves under O₂ flow (Figure S9).

The UV/vis spectra demonstrate that these three isostructural MOFs show very broad absorption throughout the region of 450–800 nm, indicating their potential to be catalyst used in photocatalysis (Figure 2b). To clarify the semiconductor properties of these MOFs and the possibility of subsequent photoreduction of CO₂, Mott–Schottky measurements were performed at frequencies of 500, 1000, and 1500 Hz. The results indicate that these three MOFs are typical n-type semiconductors (Figure 2c, and Figures S10 and S11). Because the intersection point is independent of the frequency, the flat positions of MOF-Ni, MOF-Co, and MOF-Cu are determined to be -1.14 , -1.34 , and -1.28 V vs Ag/AgCl, respectively. Thus, the bottom of the conduction band (LUMO) of MOF-Ni, MOF-Co, and MOF-Cu are estimated to be -0.94 , -1.14 , and -1.08 V vs the normal hydrogen electrode (NHE), respectively.⁵¹ From the Tauc plot, the band gaps of the MOF-

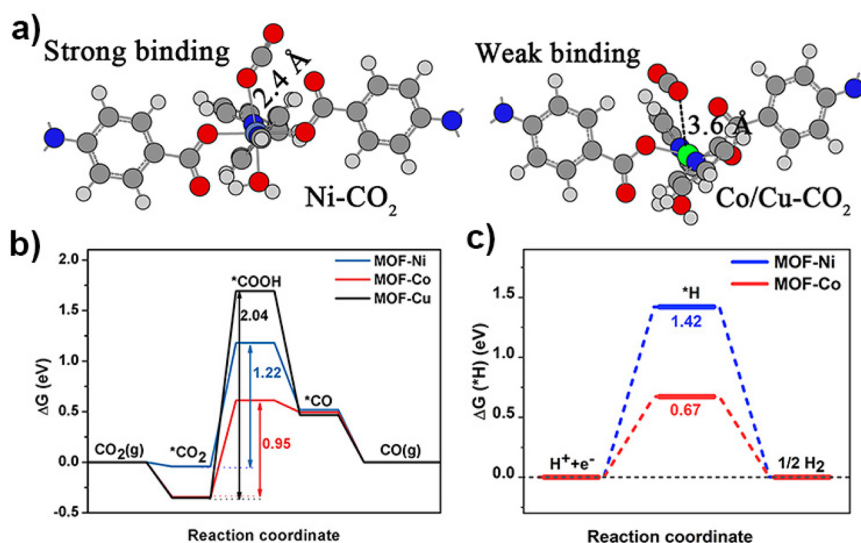


Figure 4. (a) Geometry structures of CO₂ adopted on three metal sites; the Ni is present as dark blue and Co/Cu are in green. (b) Free energy profile of CO₂RR toward the production of CO. (c) Free energy diagram of HER.

Ni, MOF-Co, and MOF-Cu were estimated to be 1.50, 2.02, and 1.77 eV by Kubelka–Munk (KM) method (Figures S12–S14). Then the valence band (HOMO) positions of these three MOFs were calculated to be 0.56, 0.88, and 0.69 eV versus NHE, respectively. Because their LUMO positions are more negative than the reduction potentials of CO₂ to many products, it is theoretically feasible to use these MOFs as catalysts for photoreducing CO₂.^{12,52} Additionally, the adsorption of CO₂ is often believed to play a crucial role in the catalytic performance of catalyst, so the volumetric CO₂ adsorption measurements were performed on the activated samples at 298 K.^{53,54} As shown in Figure 2d, the CO₂ uptakes at 298 K were found to be 40.35, 38.87, and 34.00 cm³ g⁻¹ for MOF-Co, MOF-Ni, and MOF-Cu, respectively.

Taking the above features of these MOFs into consideration, the photocatalytic CO₂RR was conducted under a pure CO₂ (1.0 atm, 298 K) atmosphere in a mixed solution of MeCN/H₂O (13:1) with triisopropanolamine (TIPA) as an electron donor. Besides, [Ru(bpy)₃]Cl₂·6H₂O (bpy = 2',2'-bipyridine) as an auxiliary photosensitizer (PS) was added into the reaction system for increasing visible-light absorption.^{12,55} Because of the matched LUMO positions between the PS and MOF-based catalysts (Figures S15–S17), photogenerated electrons were allowed to migrate from the PS to the MOFs.^{56,57} On the basis of the different optical and electrochemical properties of these isomorphous MOFs, their differences in the performance of CO₂RR can be demonstrated through a series of photocatalytic experiments. As shown in Figure 3a, increasing the generation of CO (22.3 μmol, i.e., 371.6 μmol g⁻¹ h⁻¹) rather than H₂ (0.5 μmol, i.e., 8.3 μmol g⁻¹ h⁻¹) were observed when reducing CO₂ with MOF-Ni as a photocatalyst under visible-light irradiation (λ ≥ 420 nm) (Figure 3b). By contrast, MOF-Co displayed a dramatic increase in the production of CO (22.8 μmol, i.e., 1140.0 μmol g⁻¹ h⁻¹) and H₂ (25.3 μmol, i.e., 1265.0 μmol g⁻¹ h⁻¹), while only 1.7 μmol (i.e., 68.0 μmol g⁻¹ h⁻¹) of CO and 5.8 μmol (i.e., 232.0 μmol g⁻¹ h⁻¹) of H₂ was shown by MOF-Cu in the same reaction system. The TONs of these photocatalytic systems are summarized in Table S3. Remarkably, the MOF-Ni exhibits a higher selectivity of CO over H₂ (97.7%) than MOF-Co (47.4%) and MOF-Cu (22.6%). Furthermore,

among the reported heterogeneous MOF-based catalysts used in the photocatalytic CO₂RR, one that exhibited such a high selectivity toward CO have been rarely seen. Gaseous CO and H₂ were the main reaction products detected by gas chromatography during the whole photocatalytic process; only trace amounts of HCOOH were produced in the aqueous solution as detected by ion chromatography.

Considering that MOF-Ni has better catalytic activity and selectivity than MOF-Cu and MOF-Co in photocatalytic CO₂RR, a series of reference experiments with MOF-Ni as the example were conducted to determine the important role of the catalyst and the experimental results are summarized in Table S3. The production of CO has a high selectivity of 97.7% over competing H₂ generation after 12 h of irradiation with visible light. This selectivity is the highest among most of the reported MOF-based photocatalysts for reducing CO₂ to CO (Table S4). The calculated quantum yield of the heterogeneous photocatalytic system was 5.3 × 10⁻³% under irradiation of 420 nm light (specific calculation method in the Supporting Information). To ascertain the source of the produced CO, we performed an isotopic tracing experiment by replacing CO₂ with ¹³CO₂. The ¹³CO₂ was used as the reactant under the same photocatalytic reaction condition, and then the reaction product was examined by gas chromatography-mass spectrometry. After irradiation with visible light, the peak at 1.8 min with *m/z* 29 was assigned to ¹³CO (Figure 3c). The results demonstrate that CO₂ is the main carbon source rather than the degradation of organics in the reaction. Additionally, the total production of the reaction products has no noticeable decrease after four cycles of 7 h reactions, suggesting the reservation of the original photocatalytic activity of MOF-Ni (Figure 3d). Furthermore, there was no noticeable alteration in their PXRD patterns and IR spectra obtained before and after the photocatalytic reactions, which again evidenced the structural robustness of the catalyst (Figures S23–S25).

To explore the reasons for the difference in photocatalytic activity of the three catalysts, we first assume that charge separation efficiency is an important factor.⁵⁸ As proved by the photocurrent characterization results, MOF-Ni and MOF-Co reveal obviously more efficient separation of photogenerated electron–hole pairs than MOF-Cu under the same conditions

(Figure S26). The fact is further supported by electrochemical impedance spectroscopy (EIS), which indicates that MOF-Co has the smallest radius and the lowest resistance in charge transportation, while MOF-Cu shows the biggest radius and the largest resistance among them (Figure S27). Therefore, MOF-Co and MOF-Ni possess higher charge-separation efficiency than MOF-Cu.

Density functional theory calculations are performed to understand the specific effects of different metal ion species on photoreduction of CO₂. We first investigate the binding between CO₂ and three metal ions, which plays an essential role in the selectivity and reactivity of the following catalytic reactions. As shown in Figure 4a, both Co and Cu present weak interaction with CO₂ with a long distance of 3.6 Å, while Ni and CO₂ form a strong coordination bond of 2.4 Å. The strong coupling between Ni and CO₂ is attributed to the high spin state of the Ni in an octahedral coordination, as seen in the spin density plot (Figure S30). However, the binding energy, calculated by $E_{BE}(*CO_2) = E(\text{total}) - E(5\text{-coordination}) - E(CO_2)$, is determined to be a small value because of the coupling between Ni and two O in the carboxyl group (Figure S31). Free energy pathways of CO₂ reduction to CO on the metal sites of MOFs and the intermediate structures are shown in Figure 4b and Figure S32. Among the four elementary reaction steps, the *COOH formation serves as the rate-limiting step and follows the order of Cu (2.04 eV) > Ni (1.22 eV) > Co (0.95 eV). The competition reaction of hydrogen evolution reaction (HER) is considered for comparison and the free energy diagram obtains 0.67 eV for Co and 1.42 eV for Ni, respectively (Figure 4c). The calculation results suggest that MOF-Ni presents the best selectivity among the three complexes because of the strong binding with CO₂ and high HER free energy, and both CO₂RR and HER processes can readily occur for MOF-Co. These findings are in good agreement with the aforementioned experiments.

In accordance with the above experimental results and theoretical calculations, a possible photocatalytic mechanism was proposed (Figure 5). First, the coordination water on the metal center is easily detached to form exposed metal active

site, where CO₂ molecules are adsorbed. Because the LUMO of MOF-M is lower than that of [Ru(bpy)₃]²⁺, the photo-generated electrons in the LUMO of [Ru(bpy)₃]²⁺ can be transferred to the surface of the MOF-M.^{59,60} Second, the CO₂ adsorbed on the metal active site accepts an electron to form radical CO₂^{•-} intermediate. Third, by the proton-assisted two-electron transport process, the absorbed CO₂ molecule was finally reduced to CO. Finally, the excited state of the photosensitizer was reductive quenching by the sacrificial electron donor TIPA and the generated CO detached from the catalyst surface.

In summary, three isostructural and stable transition-metal-based MOFs were synthesized and used as catalysts applied in the heterogeneous photocatalytic CO₂RR. It is significant that MOF-Ni displays a very high selectivity of 97.7% for the CO₂-to-CO conversion, which has surpassed most of the reported MOF-based catalysts in the field of CO₂RR. Furthermore, the precise and simple structural models with a single metal active site enable us to understand more definitively the specific effects of different metal-ion species on photoreduction of CO₂ and the reactive mechanism. Our findings are anticipated to providing more insights into the development of more efficient, stable and selective catalysts for photocatalytic CO₂RR.

■ ASSOCIATED CONTENT

● Supporting Information

The Supporting Information is available free of charge on the ACS Publications website at DOI: 10.1021/acscatal.8b04887.

Details of synthesis, more characterization, and theoretical calculations (PDF)

Crystallographic data for MOF-Ni (CIF)

Crystallographic data for MOF-Co (CIF)

Crystallographic data for MOF-Cu (CIF)

■ AUTHOR INFORMATION

Corresponding Authors

*E-mail: lidongsheng1@126.com (D.S.L.).

*E-mail: yqlan@njinu.edu.cn (Y.Q.L.).

ORCID

Long-Zhang Dong: 0000-0002-9276-5101

Dong-Sheng Li: 0000-0003-1283-6334

Ya-Qian Lan: 0000-0002-2140-7980

Author Contributions

#These authors contributed equally (X.-K.W. and J.L.).

Notes

The authors declare no competing financial interest.

■ ACKNOWLEDGMENTS

This work was financially supported by NSF of China (21673127) and the 111 project of Hubei Province (2018–19).

■ REFERENCES

- (1) Zhang, N.; Wang, L.; Wang, H.; Cao, R.; Wang, J.; Bai, F.; Fan, H. Self-Assembled One-Dimensional Porphyrin Nanostructures with Enhanced Photocatalytic Hydrogen Generation. *Nano Lett.* **2018**, *18*, 560–566.
- (2) Kim, W.; McClure, B. A.; Edri, E.; Frei, H. Coupling carbon dioxide reduction with water oxidation in nanoscale photocatalytic assemblies. *Chem. Soc. Rev.* **2016**, *45*, 3221–3243.

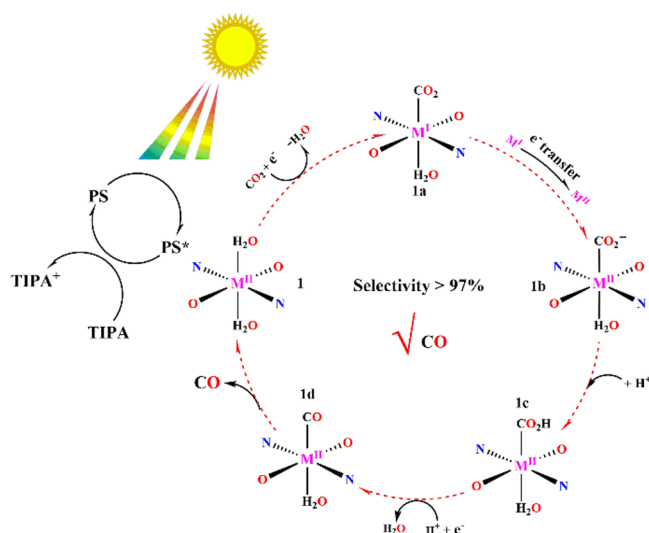


Figure 5. Proposed photocatalytic mechanism of MOFs for the CO₂ to CO conversion.

- (3) Listorti, A.; Durrant, J.; Barber, J. Artificial photosynthesis: solar to fuel. *Nat. Mater.* **2009**, *8*, 929.
- (4) Tu, W.; Zhou, Y.; Zou, Z. Photocatalytic conversion of CO₂ into renewable hydrocarbon fuels: state-of-the-art accomplishment, challenges, and prospects. *Adv. Mater.* **2014**, *26*, 4607–4626.
- (5) Zong, X.; Han, J.; Seger, B.; Chen, H.; Lu, G.; Li, C.; Wang, L. An integrated photoelectrochemical–chemical loop for solar-driven overall splitting of hydrogen sulfide. *Angew. Chem., Int. Ed.* **2014**, *53*, 4399–4403.
- (6) Diercks, C. S.; Liu, Y.; Cordova, K. E.; Yaghi, O. M. The role of reticular chemistry in the design of CO₂ reduction catalysts. *Nat. Mater.* **2018**, *17*, 301–307.
- (7) Habisreutinger, S. N.; Schmidt-Mende, L.; Stolarczyk, J. K. Photocatalytic reduction of CO₂ on TiO₂ and other semiconductors. *Angew. Chem., Int. Ed.* **2013**, *52*, 7372–7408.
- (8) Schneider, J.; Matsuoka, M.; Takeuchi, M.; Zhang, J.; Horiuchi, Y.; Anpo, M.; Bahnemann, D. W. Understanding TiO₂ photocatalysis: mechanisms and materials. *Chem. Rev.* **2014**, *114*, 9919–9986.
- (9) Xiao, F.-X.; Miao, J.; Liu, B. Layer-by-layer self-assembly of CdS quantum dots/graphene nanosheets hybrid films for photoelectrochemical and photocatalytic applications. *J. Am. Chem. Soc.* **2014**, *136*, 1559–1569.
- (10) Wu, J.; Li, X.; Shi, W.; Ling, P.; Sun, Y.; Jiao, X.; Gao, S.; Liang, L.; Xu, J.; Yan, W.; et al. Efficient Visible-Light-Driven CO₂ Reduction Mediated by Defect-Engineered BiOBr Atomic Layers. *Angew. Chem., Int. Ed.* **2018**, *57*, 8719–8723.
- (11) Gao, C.; Meng, Q.; Zhao, K.; Yin, H.; Wang, D.; Guo, J.; Zhao, S.; Chang, L.; He, M.; Li, Q.; et al. Co₃O₄ Hexagonal Platelets with Controllable Facets Enabling Highly Efficient Visible-Light Photocatalytic Reduction of CO₂. *Adv. Mater.* **2016**, *28*, 6485–6490.
- (12) Tong, H.; Ouyang, S.; Bi, Y.; Umezawa, N.; Oshikiri, M.; Ye, J. Nano-photocatalytic materials: possibilities and challenges. *Adv. Mater.* **2012**, *24*, 229–251.
- (13) Kuriki, R.; Sekizawa, K.; Ishitani, O.; Maeda, K. Visible-light-driven CO₂ reduction with carbon nitride: enhancing the activity of ruthenium catalysts. *Angew. Chem., Int. Ed.* **2015**, *54*, 2406–2409.
- (14) Wang, M.; Chen, L.; Lau, T. C.; Robert, M. A Hybrid Co Quaterpyridine Complex/Carbon Nanotube Catalytic Material for CO₂ Reduction in Water. *Angew. Chem., Int. Ed.* **2018**, *57*, 7769–7773.
- (15) Wang, S.; Guan, B. Y.; Lu, Y.; Lou, X. W. D. Formation of hierarchical In₂S₃–CdIn₂S₄ heterostructured nanotubes for efficient and stable visible light CO₂ reduction. *J. Am. Chem. Soc.* **2017**, *139*, 17305–17308.
- (16) Kuriki, R.; Ichibha, T.; Hongo, K.; Lu, D.; Maezono, R.; Kageyama, H.; Ishitani, O.; Oka, K.; Maeda, K. A Stable, Narrow-Gap Oxyfluoride Photocatalyst for Visible-Light Hydrogen Evolution and Carbon Dioxide Reduction. *J. Am. Chem. Soc.* **2018**, *140*, 6648–6655.
- (17) Yuan, S.; Feng, L.; Wang, K.; Pang, J.; Bosch, M.; Lollar, C.; Sun, Y.; Qin, J.; Yang, X.; Zhang, P.; et al. Stable Metal–Organic Frameworks: Design, Synthesis, and Applications. *Adv. Mater.* **2018**, *30*, 1704303.
- (18) Wu, X. Q.; Zhao, J.; Wu, Y. P.; Dong, W. W.; Li, D. S.; Li, J. R.; Zhang, Q. Ultrafine Pt Nanoparticles and Amorphous Nickel Supported on 3D Mesoporous Carbon Derived from Cu–Metal–Organic Framework for Efficient Methanol Oxidation and Nitrophenol Reduction. *ACS Appl. Mater. Interfaces* **2018**, *10*, 12740–12749.
- (19) Li, F. L.; Shao, Q.; Huang, X.; Lang, J. P. Nanoscale Trimetallic Metal–Organic Frameworks Enable Efficient Oxygen Evolution Electrocatalysis. *Angew. Chem., Int. Ed.* **2018**, *57*, 1888–1892.
- (20) Hao, J.; Xu, X.; Fei, H.; Li, L.; Yan, B. Functionalization of Metal–Organic Frameworks for Photoactive Materials. *Adv. Mater.* **2018**, *30*, 1705634.
- (21) Zhou, W.; Wu, Y. P.; Zhao, J.; Dong, W. W.; Qiao, X. Q.; Hou, D. F.; Bu, X.; Li, D. S. Efficient Gas-Sensing for Formaldehyde with 3D Hierarchical Co₃O₄ Derived from Co₅-Based MOF Microcrystals. *Inorg. Chem.* **2017**, *56*, 14111–14117.
- (22) Zhang, F. M.; Dong, L. Z.; Qin, J. S.; Guan, W.; Liu, J.; Li, S. L.; Lu, M.; Lan, Y. Q.; Su, Z. M.; Zhou, H. C. Effect of imidazole arrangements on proton-conductivity in metal–organic frameworks. *J. Am. Chem. Soc.* **2017**, *139*, 6183–6189.
- (23) Wu, Y. P.; Zhou, W.; Zhao, J.; Dong, W. W.; Lan, Y. Q.; Li, D. S.; Sun, C.; Bu, X. Surfactant-Assisted Phase-Selective Synthesis of New Cobalt MOFs and Their Efficient Electrocatalytic Hydrogen Evolution Reaction. *Angew. Chem., Int. Ed.* **2017**, *56*, 13001–13005.
- (24) Trickett, C. A.; Helal, A.; Al-Maythaly, B. A.; Yamani, Z. H.; Cordova, K. E.; Yaghi, O. M. The chemistry of metal–organic frameworks for CO₂ capture, regeneration and conversion. *Nat. Rev. Mater.* **2017**, *2*, 17045.
- (25) Li, X. X.; Shen, F. C.; Liu, J.; Li, S. L.; Dong, L. Z.; Fu, Q.; Su, Z. M.; Lan, Y. Q. A highly stable polyoxometalate-based metal–organic framework with an ABW zeolite-like structure. *Chem. Commun.* **2017**, *53*, 10054–10057.
- (26) Chen, Y. C.; Liu, J. L.; Wernsdorfer, W.; Liu, D.; Chibotaru, L. F.; Chen, X. M.; Tong, M. L. Hyperfine-Interaction-Driven Suppression of Quantum Tunneling at Zero Field in a Holmium (III) Single-Ion Magnet. *Angew. Chem., Int. Ed.* **2017**, *56*, 4996–5000.
- (27) Li, B.; Wen, H. M.; Cui, Y.; Zhou, W.; Qian, G.; Chen, B. Emerging multifunctional metal–organic framework materials. *Adv. Mater.* **2016**, *28*, 8819–8860.
- (28) Hou, B. L.; Tian, D.; Liu, J.; Dong, L. Z.; Li, S. L.; Li, D. S.; Lan, Y. Q. A water-stable metal–organic framework for highly sensitive and selective sensing of Fe³⁺ ion. *Inorg. Chem.* **2016**, *55*, 10580–10586.
- (29) Zhang, W.; Li, R.; Zhao, X.; Chen, Z.; Law, A. W.-K.; Zhou, K. A Cobalt-Based Metal–Organic Framework as Cocatalyst on BiVO₄ Photoanode for Enhanced Photoelectrochemical Water Oxidation. *ChemSusChem* **2018**, *11*, 2710–2716.
- (30) Wu, R.; Wang, D. P.; Kumar, V.; Zhou, K.; Law, A. W. K.; Lee, P. S.; Lou, J.; Chen, Z. MOFs-derived copper sulfides embedded within porous carbon octahedra for electrochemical capacitor applications. *Chem. Commun.* **2015**, *51*, 3109–3112.
- (31) Wu, R.; Qian, X.; Rui, X.; Liu, H.; Yadian, B.; Zhou, K.; Wei, J.; Yan, Q.; Feng, X.-Q.; Long, Y.; et al. Zeolitic imidazolate framework 67-derived high symmetric porous Co₃O₄ hollow dodecahedra with highly enhanced lithium storage capability. *Small* **2014**, *10*, 1932–1938.
- (32) Sun, M.; Yan, S.; Sun, Y.; Yang, X.; Guo, Z.; Du, J.; Chen, D.; Chen, P.; Xing, H. Enhancement of visible-light-driven CO₂ reduction performance using an amine-functionalized zirconium metal–organic framework. *Dalton Trans.* **2018**, *47*, 909–915.
- (33) Liu, J.; Fan, Y. Z.; Li, X.; Wei, Z.; Xu, Y. W.; Zhang, L.; Su, C.-Y. A porous rhodium (III)-porphyrin metal-organic framework as an efficient and selective photocatalyst for CO₂ reduction. *Appl. Catal., B* **2018**, *231*, 173–181.
- (34) Wang, S.; Yao, W.; Lin, J.; Ding, Z.; Wang, X. Cobalt imidazolate metal–organic frameworks photosplit CO₂ under mild reaction conditions. *Angew. Chem., Int. Ed.* **2014**, *53*, 1034–1038.
- (35) Zhang, T.; Lin, W. Metal–organic frameworks for artificial photosynthesis and photocatalysis. *Chem. Soc. Rev.* **2014**, *43*, 5982–5993.
- (36) Chen, Y.; Wang, D.; Deng, X.; Li, Z. Metal–organic frameworks (MOFs) for photocatalytic CO₂ reduction. *Catal. Sci. Technol.* **2017**, *7*, 4893–4904.
- (37) Wang, C.; Xie, Z.; deKrafft, K. E.; Lin, W. Doping metal–organic frameworks for water oxidation, carbon dioxide reduction, and organic photocatalysis. *J. Am. Chem. Soc.* **2011**, *133*, 13445–13454.
- (38) Wang, X.; Wissler, F. M.; Canivet, J.; Fontecave, M.; Mellot-Draznics, C. Immobilization of a Full Photosystem in the Large-Pore MIL-101 Metal–Organic Framework for CO₂ reduction. *ChemSusChem* **2018**, *11*, 3315–3322.
- (39) Wang, D.; Huang, R.; Liu, W.; Sun, D.; Li, Z. Fe-based MOFs for photocatalytic CO₂ reduction: role of coordination unsaturated sites and dual excitation pathways. *ACS Catal.* **2014**, *4*, 4254–4260.
- (40) Wang, Y.; Huang, N. Y.; Shen, J. Q.; Liao, P. Q.; Chen, X. M.; Zhang, J. P. Hydroxide Ligands Cooperate with Catalytic Centers in

Metal–Organic Frameworks for Efficient Photocatalytic CO₂ Reduction. *J. Am. Chem. Soc.* **2018**, *140*, 38–41.

(41) Ye, L.; Gao, Y.; Cao, S.; Chen, H.; Yao, Y.; Hou, J.; Sun, L. Assembly of highly efficient photocatalytic CO₂ conversion systems with ultrathin two-dimensional metal–organic framework nanosheets. *Appl. Catal., B* **2018**, *227*, 54–60.

(42) Zhao, J.; Wang, Q.; Sun, C.; Zheng, T.; Yan, L.; Li, M.; Shao, K.; Wang, X.; Su, Z. A hexanuclear cobalt metal–organic framework for efficient CO₂ reduction under visible light. *J. Mater. Chem. A* **2017**, *5*, 12498–12505.

(43) Chen, D.; Xing, H.; Wang, C.; Su, Z. Highly efficient visible-light-driven CO₂ reduction to formate by a new anthracene-based zirconium MOF via dual catalytic routes. *J. Mater. Chem. A* **2016**, *4*, 2657–2662.

(44) Yan, Z. H.; Du, M. H.; Liu, J.; Jin, S.; Wang, C.; Zhuang, G.-L.; Kong, X.-J.; Long, L.-S.; Zheng, L.-S. Photo-generated dinuclear {Eu(II)}₂ active sites for selective CO₂ reduction in a photosensitizing metal–organic framework. *Nat. Commun.* **2018**, *9*, 3353.

(45) Deng, X.; Albero, J.; Xu, L.; García, H.; Li, Z. Construction of a Stable Ru–Re Hybrid System Based on Multifunctional MOF-253 for Efficient Photocatalytic CO₂ Reduction. *Inorg. Chem.* **2018**, *57*, 8276–8286.

(46) Zhang, S.; Li, L.; Zhao, S.; Sun, Z.; Luo, J. Construction of interpenetrated ruthenium metal–organic frameworks as stable photocatalysts for CO₂ reduction. *Inorg. Chem.* **2015**, *54*, 8375–8379.

(47) Chen, E. X.; Qiu, M.; Zhang, Y. F.; Zhu, Y. S.; Liu, L. Y.; Sun, Y. Y.; Bu, X.; Zhang, J.; Lin, Q. Acid and Base Resistant Zirconium Polyphenolate-Metalloporphyrin Scaffolds for Efficient CO₂ Photo-reduction. *Adv. Mater.* **2018**, *30*, 1704388.

(48) Wen, L.; Zhao, J.; Lv, K.; Wu, Y.; Deng, K.; Leng, X.; Li, D. Visible-light-driven photocatalysts of metal–organic frameworks derived from multi-carboxylic acid and imidazole-based spacer. *Cryst. Growth Des.* **2012**, *12*, 1603–1612.

(49) Wang, F.; Ke, X.; Zhao, J.; Deng, K.; Leng, X.; Tian, Z.; Wen, L.; Li, D. Six new metal–organic frameworks with multi-carboxylic acids and imidazole-based spacers: syntheses, structures and properties. *Dalton Trans.* **2011**, *40*, 11856–11865.

(50) Cui, J. W.; Hou, S. X.; Li, Y. H.; Cui, G. H. A multifunctional Ni (II) coordination polymer: synthesis, crystal structure and applications as a luminescent sensor, electrochemical probe, and photocatalyst. *Dalton Trans.* **2017**, *46*, 16911–16924.

(51) Wang, S.; Lin, J.; Wang, X. Semiconductor–redox catalysis promoted by metal–organic frameworks for CO₂ reduction. *Phys. Chem. Chem. Phys.* **2014**, *16*, 14656–14660.

(52) Li, R.; Zhang, W.; Zhou, K. Metal–Organic-Framework-Based Catalysts for Photoreduction of CO₂. *Adv. Mater.* **2018**, *30*, 1705512.

(53) Dhakshinamoorthy, A.; Asiri, A. M.; Garcia, H. Metal–organic framework (MOF) compounds: photocatalysts for redox reactions and solar fuel production. *Angew. Chem., Int. Ed.* **2016**, *55*, 5414–5445.

(54) Zhang, H.; Wei, J.; Dong, J.; Liu, G.; Shi, L.; An, P.; Zhao, G.; Kong, J.; Wang, X.; Meng, X.; et al. Efficient Visible-Light-Driven Carbon Dioxide Reduction by a Single-Atom Implanted Metal–Organic Framework. *Angew. Chem., Int. Ed.* **2016**, *55*, 14310–14314.

(55) Ouyang, T.; Huang, H. H.; Wang, J. W.; Zhong, D. C.; Lu, T. B. A Dinuclear Cobalt Cryptate as a Homogeneous Photocatalyst for Highly Selective and Efficient Visible-Light Driven CO₂ Reduction to CO in CH₃CN/H₂O Solution. *Angew. Chem., Int. Ed.* **2017**, *56*, 738–743.

(56) Kočí, K.; Obalová, L.; Matějová, L.; Plachá, D.; Lacný, Z.; Jirkovský, J.; Šolcová, O. Effect of TiO₂ particle size on the photocatalytic reduction of CO₂. *Appl. Catal., B* **2009**, *89*, 494–502.

(57) Chen, X.; Zhou, Y.; Liu, Q.; Li, Z.; Liu, J.; Zou, Z. Ultrathin, single-crystal WO₃ nanosheets by two-dimensional oriented attachment toward enhanced photocatalytic reduction of CO₂ into hydrocarbon fuels under visible light. *ACS Appl. Mater. Interfaces* **2012**, *4*, 3372–3377.

(58) Liu, H.; Xu, C.; Li, D.; Jiang, H. L. Photocatalytic Hydrogen Production Coupled with Selective Benzylamine Oxidation over MOF Composites. *Angew. Chem., Int. Ed.* **2018**, *57*, 5379–5383.

(59) He, J.; Wang, J.; Chen, Y.; Zhang, J.; Duan, D.; Wang, Y.; Yan, Z. A dye-sensitized Pt@UiO-66(Zr) metal–organic framework for visible-light photocatalytic hydrogen production. *Chem. Commun.* **2014**, *50*, 7063–7066.

(60) Xie, S. L.; Liu, J.; Dong, L. Z.; Li, S. L.; Lan, Y. Q.; Su, Z. M. Hetero-metallic active sites coupled with strongly reductive polyoxometalate for selective photocatalytic CO₂-to-CH₄ conversion in water. *Chem. Sci.* **2019**, *10*, 185–190.